### Title

Seismic Performance of Symmetric Unfinished CFS In-Line Wall Systems




### ISBN

9780784482896



### Authors

Singh, Amanpreet
Wang, Xiang
Torabian, Shahab
et al.



### Publication Date

2020-04-02

### DOI

10.1061/9780784482896.058

# Seismic Performance of Symmetric Unfinished CFS In-Line Wall Systems

Amanpreet Singh[1]; Xiang Wang, Ph.D.[2]; Shahab Torabian, Ph.D.[3];
Tara C. Hutchinson, Ph.D., P.E.[4]; Kara D. Peterman, Ph.D.[5]; and Benjamin W. Schafer, Ph.D.[6]

[1]Graduate Student, Dept. of Structural Engineering, Univ. of California, San Diego, La Jolla, CA. E-mail: ams082@eng.ucsd.edu
[2]Post-Doctoral Researcher, Dept. of Structural Engineering, Univ. of California, San Diego, La Jolla, CA. E-mail: xiw002@eng.ucsd.edu
[3]Senior Project Consultant, Simpson Gumpertz & Heger, Washington, DC; formerly Senior Engineer, NBM Technologies Inc., Baltimore, MD. E-mail: storabian@sgh.com
[4]Professor, Dept. of Structural Engineering, Univ. of California, San Diego, La Jolla, CA. E-mail: tara@ucsd.edu
[5]Assistant Professor, Dept. of Civil and Environmental Engineering, Univ. of Massachusetts Amherst, Amherst, MA. E-mail: kdpeterman@umass.edu
[6]Professor, Dept. of Civil Engineering, John Hopkins Univ., Baltimore, MD. E-mail: schafer@jhu.edu



## ABSTRACT

The current North American standards, AISI S240 (2015) and AISI S400 (2015), provide information that can be used to design cold-formed steel (CFS) framed steel sheet shear walls which meet the seismic demands for a low-rise to mid-rise (3–6 story) buildings. However, experimental data to support code guidelines for taller mid-rise (>6 stories) and high-rise buildings (>10 stories), where large lateral load resistance is required, are lacking. Moreover, most of the experimental research so far has involved testing shear walls under quasi-static monotonic/reversed cyclic loading. In the current research project, shear walls placed in-line with gravity walls were tested at full-scale first under a sequence of increasing amplitude (in-plane) earthquake motions, and subsequently (for select specimens) under slow monotonic pull conditions to failure. Experiments were performed at the NHERI Large High-Performance Outdoor Shake Table at UC San Diego. Selection of wall details was motivated by the design of a CFS archetype building (4 and 10 story) using available experimental data. This paper explains the design details and discusses the experimental response of a baseline wall specimen pair in the test program, which uses compression chord stud packs with a steel tension tie-rods assembly, is unfinished and designed with a symmetric configuration.

## INTRODUCTION

The construction industry in North America has seen substantial growth in the use of cold-formed steel (CFS) framed construction in recent years. CFS buildings offer an effective solution for mid-rise structures with several benefits such as lightweight framing, high durability and ductility, low installation and maintenance costs (Schafer, 2011). Buildings framed with repetitively placed light gauge CFS walls develop lateral resistance through sheathing attached to the wall framing members. CFS shear walls commonly use OSB or gypsum panels as sheathing on one or both sides of the wall. Use of steel sheet as sheathing is relatively new and understanding of the structural behavior of steel sheet sheathed shear walls remains limited. Research conducted by Serrette et al. (1997), Yu (2010), Yu and Chen (2011), DaBreo et al. (2014) and Balh et al. (2014) has contributed to the development of the current North American

Standards, AISI S240 (2015) and AISI S400 (2015), providing information for designing shear walls with steel sheet sheathing.

The current design standards can be used to design CFS shear walls to meet the seismic demands for low- to mid-rise (3-6 story) buildings. However, design guidelines for mid- and high-rise buildings taller than 6 stories are lacking due to their large lateral load resistance requirements. Moreover, with perhaps only the exception of Shamin et al. (2013), very few studies have incorporated dynamic loading during their experiments on steel sheathed CFS framed shear walls. Rather most have involved testing shear walls under quasi-static monotonic/reversed cyclic loading. An additional and equally important limitation within the experimental literature is that, the previous studies have considered shear walls and gravity walls separately. However, these wall components have to work together when placed along the same line to support the architectural layout/purpose in buildings. Walls often have openings (doors and windows) and have finishes installed (exterior and interior) for insulation purposes.

In the current research project, several of these limitations are addressed in an effort to enrich the experimental database documenting the performance of CFS wall-braced components. Contrasting prior tests, shear walls are placed in-line with gravity walls and tested at full-scale first under a sequence of increasing amplitude (in-plane) earthquake motions, and subsequently under slow monotonic pull conditions to failure (for select specimens). The experimental program had the following key objectives: (a) characterize the dynamic performance of CFS walls, (b) understand the effect of finishes and openings on wall behavior, (c) compare the behavior of Type 1 and Type 2 walls, (d) compare the behavior of symmetrical and unsymmetrical walls and (e) examine lateral load sharing between shear walls placed in-line with gravity walls This paper summarizes an archetype building designed within the CFS-NHERI project, which was utilized as the basis for design details of a suite of wall line specimens tested on the NHERI@ UC San Diego shake table. Particular attention herein is given to the response results of the baseline specimen within the suite, which uses compression chord stud packs with a steel tension tie-rods assembly, is unfinished and laid out with a symmetric shear wall configuration.

## CFS-NHERI ARCHETYPE BUILDING DESIGN

CFS framing can be used as the gravity and lateral force resisting system (LFRS) for low-rise buildings, however it may need to be used in conjunction with other materials/systems such as reinforced concrete shear walls or core walls as the height of the building increases. This reduces the efficiency and favorability of CFS construction. To this end, a complete archetype building using only CFS framing helps advance new CFS detailing and evaluation of buildings constructed entirely using these systems. The archetype mid-rise CFS building discussed in Torabian et al. (2016) was used as the basis for the CFS-NHERI archetype building, using CFS framing only for entire gravity and lateral force resisting systems, including ledger framing similar to CFS-NEES building (Peterman et al., 2016). The typical floor plan of this archetype building was selected as 35.4 m × 14.6 m and is shown in Figure 1. The hypothetical site of the CFS-NHERI archetype building was located in Orange County (coordinates: 33.79˚N, -117.86˚W and site class: D). As a result, the following design parameters were assumed in accordance with ASCE 7 (ASCE 2016): spectral acceleration at short periods, $S_s$=1.39 *g*, spectral acceleration at a period of 1s, $S_1$=0.57 *g*, and design spectral accelerations, $S_{DS}$ = 0.927 *g* and $S_{D1}$ = 0.57 *g*.

The LFRS of the archetype building consisted of Type I steel sheet sheathed shear walls

anchored with tension tie-rods and compression stud packs at wall ends. The seismic design parameters R (response modification coefficient), $\Omega_o$ (over-strength factor) and $C_d$ (deflection amplification factor) for light-frame (cold-formed steel) walls sheathed with wood structural panels rated for shear resistance or steel sheets are as 6.5, 3 and 4, respectively (ASCE-7, 2016). It is noted that the current code provisions require that the structural systems of this kind are restricted to a structural height limit at 65 ft (~6 story building). Utilizing this floor plan and codified design seismic demand details, a 4-story and a 10-story CFS archetype were designed. Assumed gravity loads were 30 psf dead load and 40 psf live load for typical floor, and 20 psf dead load and 20 psf live load for roof. The effective seismic weight calculated based on estimated weights of the floor, roof and walls was 211.5 kips for a typical floor and 105.8 kips for the roof. The 4-story building, which meets the code height limitations, could be designed with existing AISI S400 steel sheet shear wall capacities. However, the 10-story building, which exceeds code height limitations, could only be designed by extending the shear wall capacities beyond AISI S400 and using available experimental data which document the larger capacity available with steel sheet sheathed shear walls (Rizk and Rogers, 2017; Santos and Rogers, 2017; Briere and Rogers, 2017). The selection of wall details for the experimental program were motivated from the design of the 10-story building. Selected shear wall details reflected the detailing from approximately the mid-height floors within the 10-story building. These wall details are highlighted in Table 1 which provides a summary of the 10-story building design. The design process highlighted current design code limitations: large compression stud packs (consisting of eight or more studs) and tight fastener spacing required in the lower floors to resist high axial and shear demands.

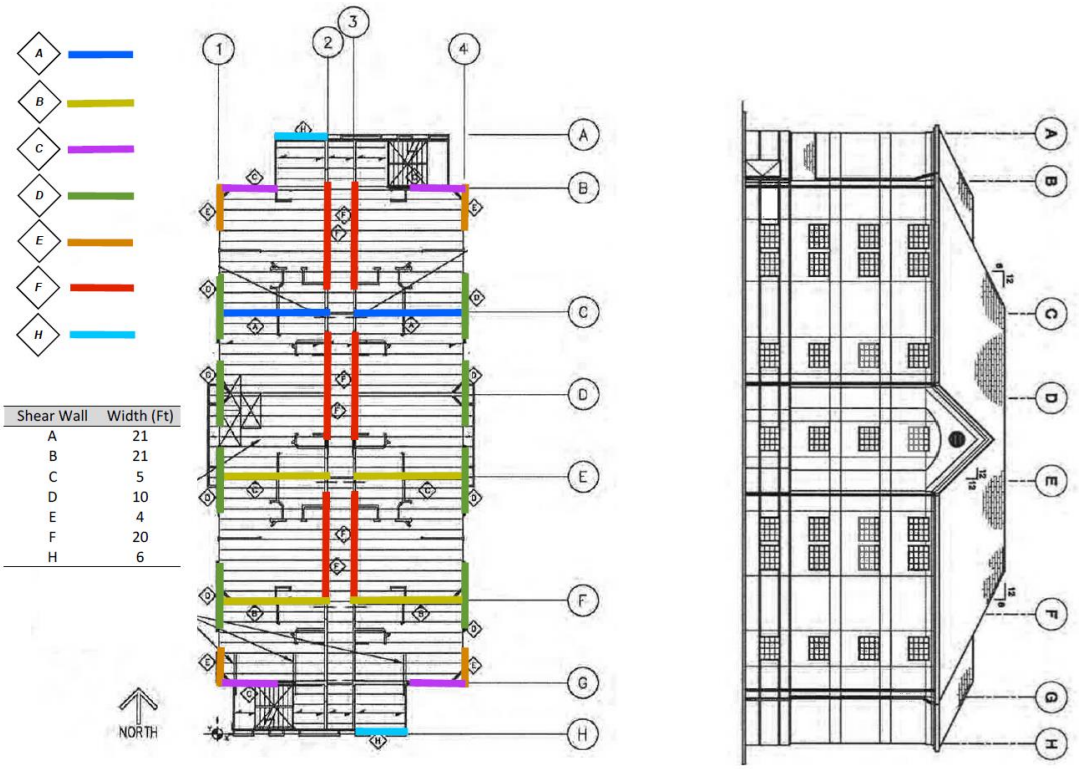


**Figure 1. The unified archetype building plan, elevation and shear wall layout (Torabian et al., 2016)**

**Table 1: Design summary: 10 story archetype building**

| | Level | Steel sheet thickness | Fastener spacing | Stud blocking | Stud pack | Chord stud | Gravity stud | Tie Rod |
|---|---|---|---|---|---|---|---|---|
| Transverse | Roof | (1) 0.027” | #8@6” | No | 2 | 600S200-54 | 600S137-33 | $\phi$0.5” |
| | 9 | (1) 0.033” | #8@3” | No | 4 | 600S200-54 | 600S137-33 | $\phi$0.75” |
| | 8 | (1) 0.033” | #8@2” | No | 4 | 600S200-97 | 600S137-33 | **$\phi$1.125”** |
| | 7 | (1) 0.030” | #10@2” | Yes | **4** | **600S250-97** | 600S137-33 | $\phi$1.375” |
| | 6 | **(1) 0.030”** | **#10@2”** | **Yes** | 6 | 600S250-97 | 600S137-33 | $\phi$1.75” |
| | 5 | (2) 0.014” | #10@2” | Yes | 6 | 600S250-97 | 600S137-33 | $\phi$2.0” |
| | 4 | (2) 0.019” | #10@2” | Yes | 6 | 600S250-97 | 600S137-33 | $\phi$2.0” |
| | 3 | (2) 0.019” | #10@2” | Yes | 10 | 600S250-97 | 600S137-43 | $\phi$2.25” |
| | 2 | (2) 0.019” | #10@2” | Yes | 10 | 600S250-97 | 600S137-43 | $\phi$3.0” |
| | 1 | (2) 0.019” | #10@2” | Yes | 12 | 600S250-97 | 600S137-43 | $\phi$3.5” |
| Longitudinal | Roof | (1) 0.018” | #8@6” | No | 2 | 600S200-43 | 600S137-33 | $\phi$0.5” |
| | 9 | (1) 0.030” | #8@6” | No | 4 | 600S200-54 | 600S250-43 | $\phi$0.75” |
| | 8 | (1) 0.033” | #8@2” | No | 4 | 600S200-68 | 600S250-54 | $\phi$1.0” |
| | 7 | (1) 0.033” | #8@2” | No | **4** | 600S250-97 | 600S250-54 | $\phi$1.375” |
| | 6 | (1) 0.033” | **#10@2”** | **Yes** | 6 | **600S250-97** | **600S250-68** | $\phi$1.75” |
| | 5 | **(1) 0.030”** | #10@2” | Yes | 6 | 600S250-97 | 600S250-68 | $\phi$2.0” |
| | 4 | (1) 0.030” | #10@2” | Yes | 6 | 600S250-97 | 600S250-68 | $\phi$2.0” |
| | 3 | (1) 0.030” | #10@2” | Yes | 10 | 600S250-97 | 600S250-97 | $\phi$2.25” |
| | 2 | (2) 0.014” | #10@2” | No | 10 | 600S250-97 | 600S250-97 | $\phi$2.75” |
| | 1 | (2) 0.014” | #10@2” | No | 10 | 600S250-97 | 600S250-97 | $\phi$3.0” |

Note: Highlighted terms indicate the selected wall details.

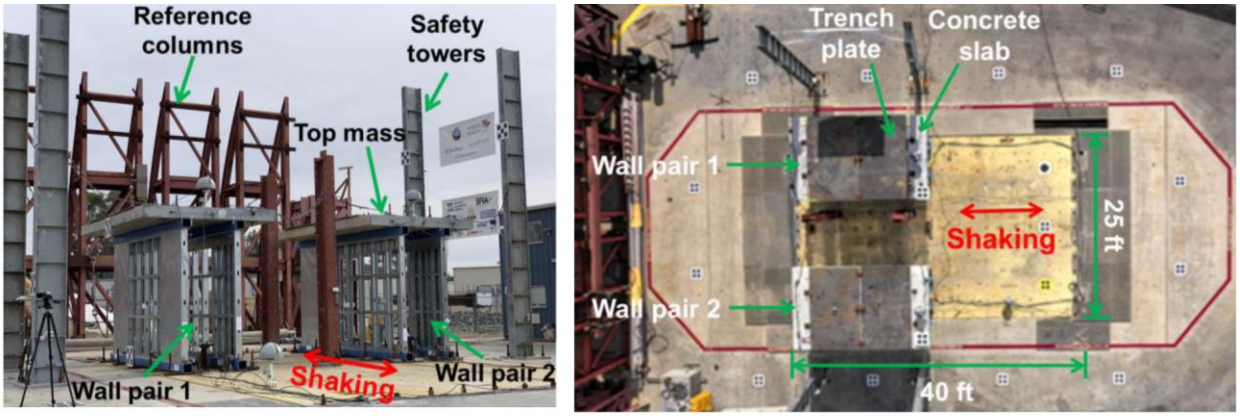


(a) (b)

**Figure 2. (a) Isometric view and (b) Top view of the test setup**

## EXPERIMENTAL PROGRAM

The CFS-NHERI wall line shake table test program consisted of 16 wall specimens tested at LHPOST at UCSD. Figure 2 shows an isometric and top view of the test setup. The shake table footprint of 12.2 m × 7.6 m (40 ft × 25 ft) allowed for two pairs of nominally identical walls to

be tested simultaneously. It is noted that the earthquake input motions were applied in the east-west direction using the single axis shake table, which aligned with the long axis of the wall specimens. The specimens were attached to top and bottom hollow steel section transfer beams using two rows of 12.7 mm (0.5 in) A325 shear bolts. These transfer beams were then attached to the shake table and mass, respectively. Figure 3 shows the locations of the drilled holes in top and bottom track for connection between specimen and transfer beams. The seismic weight for the wall pair consisted of a concrete slab (5.0 m × 3.0 m × 254 mm, 16.5 ft × 10 ft × 10 in), two steel plates (1.8 m × 3.0 m × 38 mm, 6 ft × 10 ft × 1.5 in) and the top transfer beams themselves, resulting in a total weight of 14.6 kN/m (1000 plf) per wall. The two pair of specimens to be tested simultaneously were selected such that they had similar expected peak strength and initial stiffness. This was done to ensure that the scaled earthquake motions subjected the two wall pairs to the same target performance level

Figure 3 shows the front view of the baseline wall specimen (SGGS-1) installed in the test setup and its framing details. In this suite, it is noted that the specimen name refers to the characteristic of a quadrant length of the specimen appended with the type of wall pair (either Type I or Type II), thus, the baseline specimen SGGS-1 is a Shear-Gravity-Gravity-Shear wall line with a Type I tie-rod (symmetric at shear wall ends) specimen. The dimensions of the individual walls were 4.88 m (16 ft) length and 2.74 m (9 ft) height. The baseline specimen was a symmetric, unfinished wall with a 2.44 m (8 ft) gravity wall segment in the middle and 1.22 m (4 ft) Type I shear wall segments on each end. Each shear wall segment was detailed with a pair of tie-down assemblies consisting of compression stud packs built up by welding toe-to-toe 600S250-97 studs and a $\phi$29 mm ($\phi$1.125”) Grade B7 tension tie rod in the middle of the stud packs on each end. The wall sheathing was made of 0.76 mm (0.030”) thick steel sheet with a nominal yield strength of 230 MPa (33 ksi). The steel sheet was attached to the shear wall framing using No. 12 flat pan head screws at 51 mm (2”) o.c edge and 305 mm (12”) o.c field spacing. The gravity wall framing utilized 600S250-68 vertical studs placed at 610 mm (2 ft) o.c. The top and bottom tracks used 600T250-97 members. Additionally, a 1200T250-97 ledger track was attached to the top 0.3 m (12”) height of the wall on the rear side. Pieces of chord stud material was used as blocking and 64 mm (2.5") wide, 1.4 mm (0.054”) thick flat strap was used for bracing. All framing members had 345 MPa (50 ksi) nominal strength and were assembled using No. 10 flat pan head screws. It should be noted that another wall pair was tested simultaneously with the baseline specimen pair, however its response is not the subject of the present paper.

The two pairs of wall specimens were densely instrumented with more than 120 analog sensors and an array of 15 cameras to record the wall responses during the tests. The analog sensors included: (a) accelerometers measuring top mass and shake table accelerations, (b) string potentiometers measuring top mass and table displacements as well as wall sheathing panel shear distortion, (c) strain gages measuring tension tie-rod and bottom HSS transfer beam strains, and (d) linear potentiometers measuring wall uplift and mass-transfer beam and wall-transfer beam slippage. All analog sensors were connected to a multi-node distributed data acquisition system that sampled data at a rate of 256 Hz. Additionally, a Global Positioning System (GPS) system and remote sensing equipment, including unmanned aerial vehicles (UAVs) and light ranging and detection (LiDAR) system, were employed to collect data during the construction and testing phases.

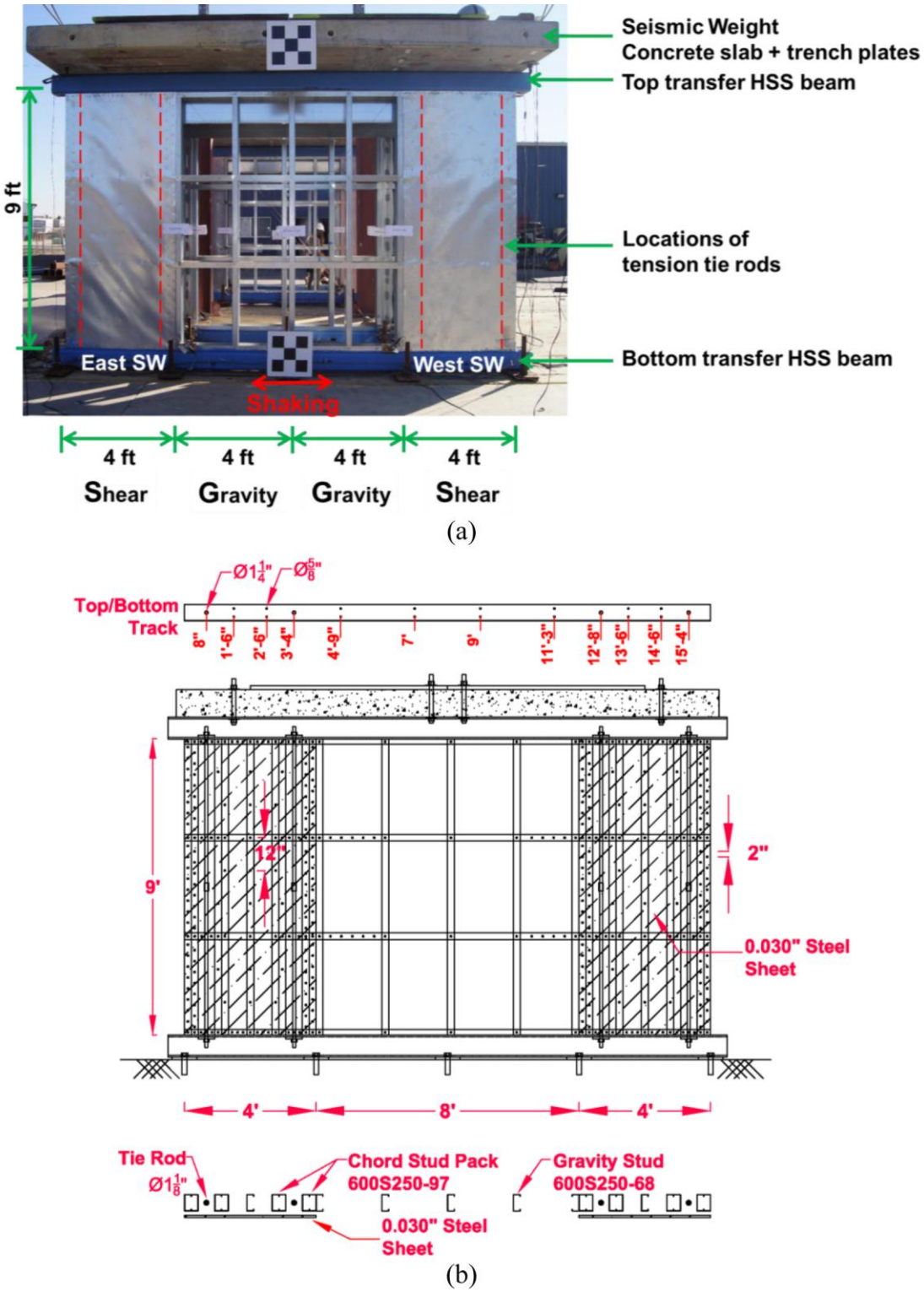


**Figure 3. (a) Baseline specimen (SGGS-1) photograph as installed in test setup and (b) framing details**

The wall specimens were tested under a sequence of increasing intensity (in-plane) earthquake motions, and subsequently, for select specimens, under slow monotonic pull

conditions until a 40% post-peak strength degradation. Two test motions from two earthquake events, namely the: (a) 1994 $M_w$=6.7 Northridge earthquake (Canoga Park record component ID: CNP196) and (b) 2010 $M_w$=8.8 Maule earthquake in Chile (Curicó record component ID: CUR-EW) were selected as seed motions guided by the objectives of including motions representative of strong earthquakes in California and including events with long durations of strong shaking (Hutchinson et al., 2017). The characteristics of the selected seed motions are shown in Figure 4. Complementing the earthquake test sequence, low-amplitude white noise tests with root mean square (RMS) intensities of 1.5%*g* and 3%*g* and durations of 3 minutes were conducted before and after each earthquake test to determine the dynamic characteristics of the wall specimens at different stages of the earthquake sequence.

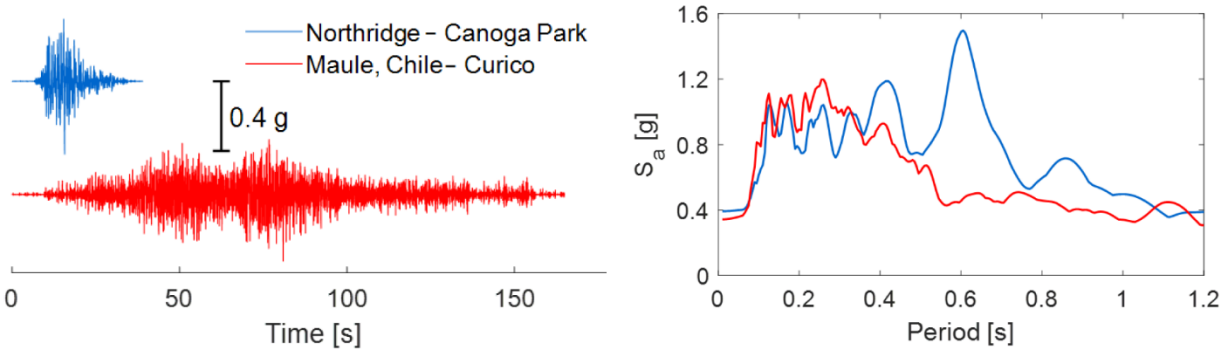


**Figure 4. Selected earthquake seed motions: (a) acceleration time histories and (b) pseudo-acceleration spectra (ξ = 5%)**

Scaling of the seed motions aimed to achieve the intended target performance levels that progressively damage the wall specimens (see Table 2). The motion scaling procedure was carried out using the following steps:

1. Determine scale factor ($SF_{desired}$) for a desired performance level using pre-test benchmark model prediction results (see Table 2).
2. Calculate performance adjustment coefficient ($SF_1$) based on selected performance level and specific On-Line Iterations (OLI) motion ($SF_{OLI}$). These OLI motions are motion iterations conducted on bare table platen until convergence on desired target of scale factors of seed motion is achieved.

$$SF_1 = SF_{desired} / SF_{\mathrm{OLI}}$$

3. Calculate motion spectra adjustment coefficient (SF2) based on achieved (or estimated) period of specimen at different damage stages during the test sequence.

$$SF_2 = \tilde{S}_{a,target} / \tilde{S}_{a,\mathrm{OLI}}$$

where $\tilde{S}_{a,target}$ and $\tilde{S}_{a,\mathrm{OLI}}$ are average spectral acceleration of the scaled seed motion and achieved bare table motion within the period interval of interest. This period interval of interest is determined using the natural period identified from a 3% *g* RMS white-noise conducted before the earthquake test and an estimated earthquake induced period elongation. For elastic and quasi-elastic performance level tests, period interval of interest was chosen as $T_1 - \alpha T_1$, where $T_1$ is the natural period of the undamaged wall specimen and $\alpha = 1.25$. For design performance level test, period interval of interest was chosen as $T_2 - \beta T_1$, where $T_2$ is the natural period of the damaged wall specimen

identified from the white noise test conducted before the design level earthquake test and $\beta = 2.0$.

4. Compute final adjusted coefficient ($SF_{final}$). This coefficient was applied to the selected OLI motion and input to the shake table to achieve the desired target performance level.

$$SF_{final} = SF_1 \times SF_2$$

Based on the defined scaling procedure, four earthquake motions with increasing intensity were selected for the baseline specimen. Table 3 summarizes the motion scale factors used for the baseline specimen earthquake test sequence. The achieved motion peak ground acceleration and peak ground displacement are listed in Table 3. The proposed procedure provided effective estimation of the scale factors for achieving the intended performance levels, with less than 10% deviation from strength targets and less than 25% deviation from drift targets. This divergence stems from the input parameters used in the force-displacement backbone definition in the benchmark models.

**Table 2: Target performance table**

| Target performance level | Response characteristics | Strength target, $V_{target}$ (% $V_{max}$) | Drift target, $\delta_{target}$ (% $\delta_{Vmax}$) | Damage |
|---|---|---|---|---|
| Elastic | Linear | 20%-40% | ~20% | Minimal damage |
| Quasi-elastic | Essentially linear | 60%–70% | 30%–40% | Minor (cosmetic) damage |
| Design | Non-linear | Near peak strength | 75%–95% | Moderate damage |
| Above design (optional) | Salient pinching | < 20% strength deterioration | 125%–150% | Continued damage, uncompromised structural integrity |

**Table 3: Selected test motions for baseline specimen**

| Test motion | Target performance level | Motion ID | $SF_{desired}$ | PGA ($g$) | PGD (cm) |
|---|---|---|---|---|---|
| EQ1: CNP196 | Elastic | EQ1:E1 | 0.64 | 0.31 | 7.69 |
| EQ2: CUR-EW | Elastic | EQ2:E2 | 0.64 | 0.24 | 2.32 |
| EQ3: CNP196 | Quasi-elastic (QE) | EQ3:QE | 1.35 | 0.66 | 17.66 |
| EQ4: CNP196 | Design event (DE) | EQ4:DE | 2.5 | 1.20 | 35.0 |

## RESULTS AND DISCUSSION

### Measured Specimen Response

The baseline specimen SGGS-1 was subjected to four earthquake input motions with increasing intensity (Table 3) as well as a sequence of low amplitude white noise tests before and after each earthquake test. At the completion of the dynamic test sequence, the wall specimens were subjected to static monotonic displacement loading test until the attainment of ultimate failure. Figure 5 shows the force-displacement responses of the wall specimen during the earthquake tests and the subsequent monotonic pull test. The force-displacement response of the specimen was essentially in the linear regime for the first three earthquake tests, since the achieved drift ratio was less than 0.4% and shear force less than 50% of its strength. The specimen behaved non-linearly during the design earthquake test as the drift demand reached 1% and shear force attained ~85% strength. During the monotonic pull test, the specimen reached its peak strength of 160.2 kN (36.0 kip) at a drift ratio of 1.95% and during continued pull demonstrated a post-peak degradation of 40% at 4.15% drift ratio. Additionally, a residual drift

of 1.85% occurred at the end of the test as the lateral force was removed. The elastic stiffness of the specimen was measured as 98.4 kN/cm (56.2 kip/in) from the white noise test in the undamaged state before the first earthquake test. The progression of damage also manifests in evolution of the period and damping. Figure 6 compares the period and damping ratio of the specimen identified at different stages using the 3%*g* RMS white noise tests conducted before and after each earthquake test. The specimen period elongated from 0.15s in its undamaged state to 0.2s after the design earthquake test (EQ4:DE). Similarly, damping increased from 2% in its undamaged state to 5% after the design earthquake test (EQ4:DE).

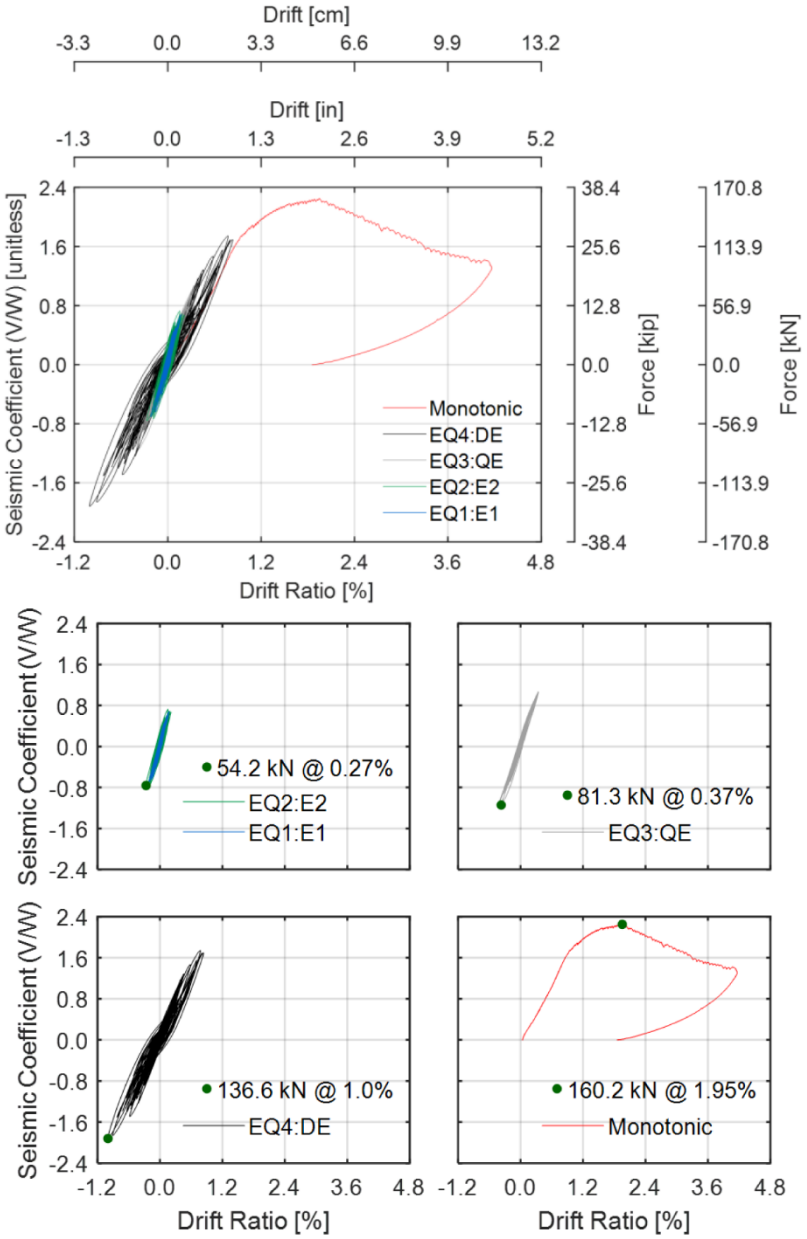


**Figure 5. Individual force-displacement response of baseline specimen (SGGS-1)**

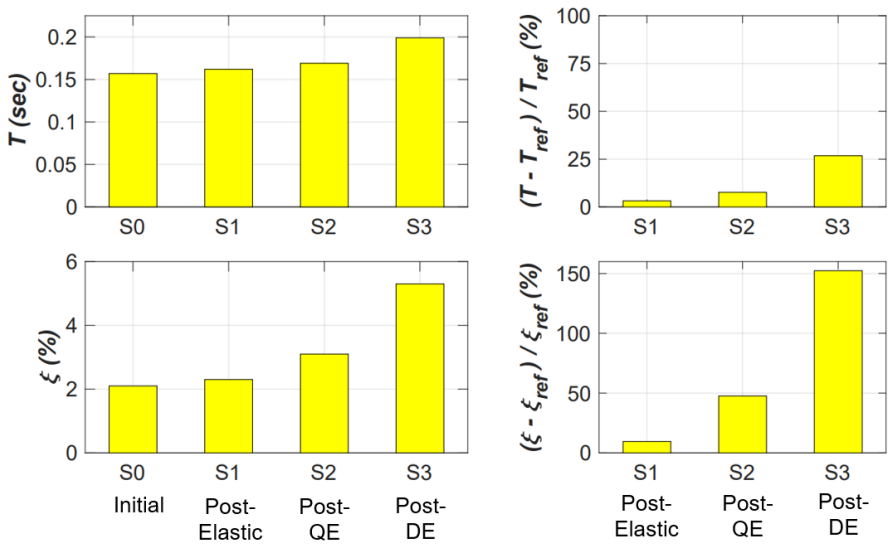


**Figure 6. Evolution of period and damping ratio at different stages of test sequence**

## Physical Damage Observations

Physical damage to the wall specimen were incipient and limited during the elastic and quasi-elastic level earthquake tests as the walls underwent low drift demands (<0.4%). Nonetheless, transient elastic sheet buckling could be observed developing within the tension field during the dynamic shaking. Damage continued to develop during the design earthquake test where drift demands reached 1%. Inelastic buckling of the steel sheet became more distributed and fastener bearing onto the steel sheet was observed. Extensive shear buckling of the sheet was observed during the monotonic pull test as drift demand increased. This was followed by partial/complete screw pull through and sheet tearing at ~2% drift. Local buckling of the gravity stud adjacent to the shear segment compression stud pack at diagonally opposite locations of the gravity wall segment was also observed during the monotonic pull test. However, the compression stud packs or track framing members did not experience any visible damage at the completion of the pull test. Photographs documenting these physical damage observations are shown in Figure 7.

## Shear Wall Measured Response

A pair of two vertical and two diagonal string potentiometers in a double-triangle configuration were used to evaluate the wall shear distortion by measuring the change in angles of the triangles. In addition, a pair of strain gages installed on the tension rods were used to calculate axial forces of the tension tie-rods. It is noted that the tensile force demands of the tension rods remained well below (<30%) their theoretical yield strength (442 kN) during the test sequence. Wall end uplift relative to the bottom HSS transfer beam was measured using linear potentiometers placed at the base of the wall at each end. Figure 8 shows these wall local responses for the design earthquake motion (EQ4:DE). The measured shear distortion of different segments of the wall matched well with the measured drift in both positive (eastward) and negative (westward) directions (red and blue circles represent the time instance when the global drift response attained the peak values in positive or negative direction). As the drift peaked in the eastward direction, the wall uplift response on the west end achieved its peak while the east end was subjected to compressive axial loads. Similarly, when wall drift peaked in

westward direction, uplift response on the east end achieved its peak and the west end showed a little compression. The response of tension tie-rods was also similar with respect to wall drift in the positive and negative direction. It was also observed that time instances of peak measurement for displacement derived response (shear distortion and uplift) matched with global drift measurement, while time instances of peak measurement for force derived response (tension rod axial force) matched better with accelerometer/shear force measurement. Tension rods placed closer to the ends of walls (exterior tie rods) consistently showed higher axial forces as compared to rods placed interior of the walls (see Figures 3 and 8). This showed that the two shear segments did not behave strictly as individual Type I walls. This observation is not consistent with the tension down rod behavior as observed in a prior full-scale building shake table test program (Wang et al., 2018). This discrepancy may be attributed to the different wall boundary elements in the two test programs. Namely, in the present program, the concrete mass at the top of the in-line wall specimens essentially act as a rigid floor diaphragm. In contrast, a CFS floor system in the building tests of Wang et al. (2018) offer nominal diaphragm flexibility. It is also noted that the tension rods experienced pre-tension loss due to repetitive shaking. The rods begin pre-tensioned, and due to the seismic motion, lose some of this pre-tension during the test. This can be seen in Figure 8, specifically examining axial force migration before and after the seismic motions.

**Figure 7. Damage observations following the monotonic pull test**

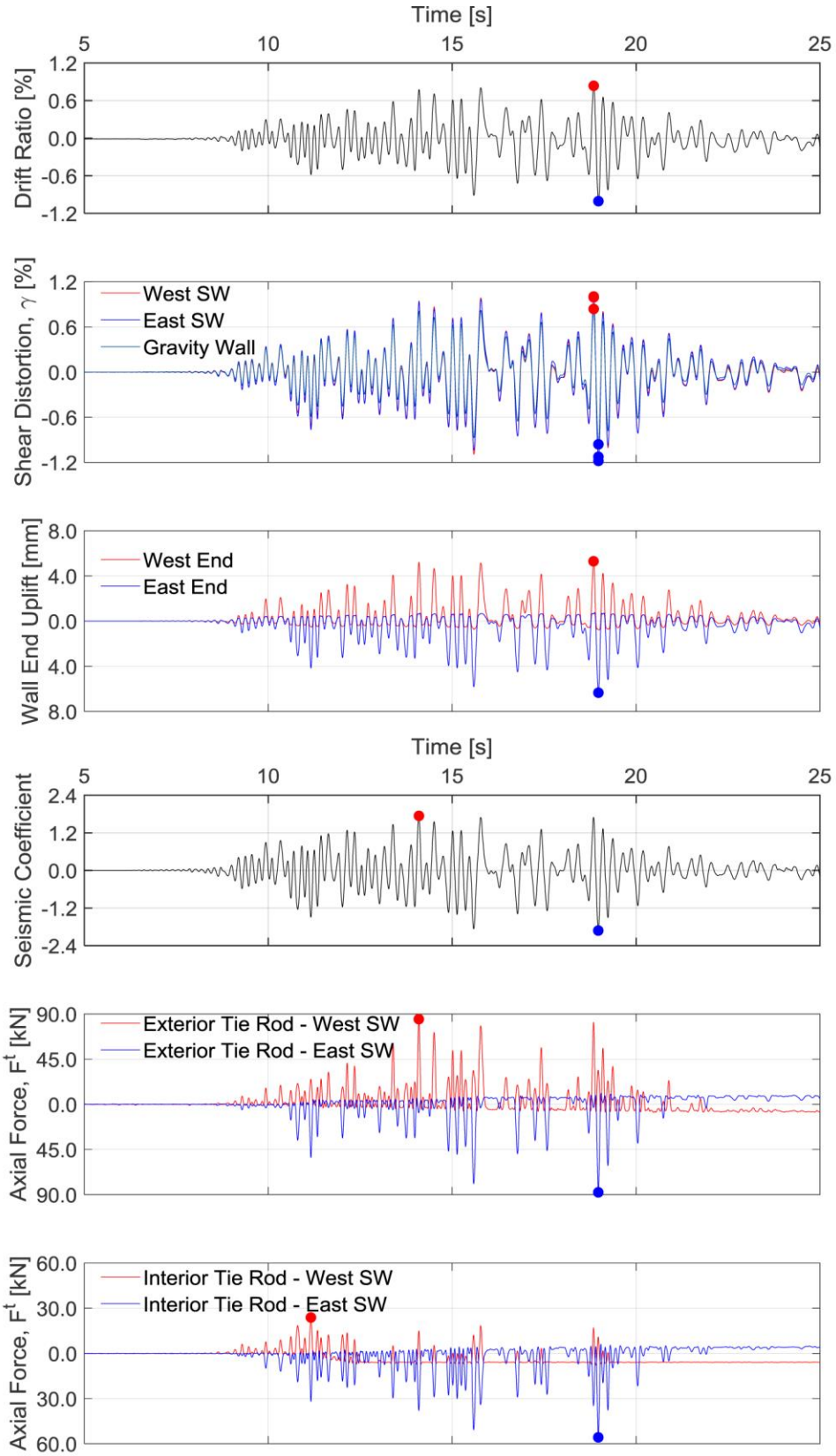


**Figure 8. Baseline specimen (SGGS-1) local response during the design earthquake test (EQ4: DE)**

## CONCLUSIONS

To advance the understanding of CFS framed steel sheet sheathed shear walls placed in line with gravity walls, full-scale specimens were tested first under a sequence of earthquake motions, and subsequently under slow monotonic pull conditions to 40% post-peak strength degradation. Selection of wall details for the experimental program were based on the design of a pair of low and mid-rise archetype buildings. The measured response of the baseline wall specimen, constructed using compression chord stud packs with a steel tension tie-rods assembly, is discussed in this paper. The specimen behaved linearly under the low drift demands imposed by the first three earthquake tests but became non-linear during the design earthquake with the drift demand reaching 1%. The specimen reached its strength of 160.2 kN at a drift ratio of 1.95% under the monotonic static displacement loading test. The progression of damage correlates well with the period and damping evolution measured during the test sequence. Physical observations showed that the specimen failed by screw pull through and sheet tearing after extensive steel sheet shear buckling at high drift demands. The axial forces in the tension-tie rods remained well below their yield strength with a margin against yield of approximately 3. No visible damage to the chord stud packs was observed after specimen failure, highlighting the effectiveness of compression chord stud packs with tension tie-rods assembly for ensuring good seismic performance of the wall-line systems.

## ACKNOWLEDGMENTS

The research presented is funded through the National Science Foundation (NSF) grants CMMI 1663569 and CMMI 1663348, project entitled: Collaborative Research: Seismic Resiliency of Repetitively Framed Mid-Rise Cold-Formed Steel Buildings. Ongoing research is a result of collaboration between three academic institutions: University of California, San Diego, Johns Hopkins University and University of Massachusetts Amherst, two institutional granting agencies: American Iron and Steel Institute and Steel Framing Industry Association and ten industry partners. Industry sponsors include ClarkDietrich Building Systems, California Expanded Metal Products Co. (CEMCO), SWS Panel and several others who each provided financial, construction, and materials support. Regarding support for the test program, the efforts of NHERI@UCSD staff, namely, Robert Beckley, Darren McKay, Jeremy Fitcher, and Alex Sherman, and graduate student Filippo Sirotti are greatly appreciated. Findings, opinions, and conclusions are those of the authors and do not necessarily reflect those of the sponsoring organizations.

## REFERENCES

AISI-S240-15 (2015). North American Standard for Cold-Formed Steel Structural Framing. American Iron and Steel Institute: Washington, D.C.

AISI-S400-15 (2015). North American Standard for Seismic Design of Cold-Formed Steel Structural Systems. American Iron and Steel Institute: Washington, D.C.

ASCE. (2016). “ASCE 7: Minimum Design Loads for Buildings and Other Structures.” ASCE Standard. American Society of Civil Engineers.

Balh, N., DaBreo, J., Ong-Tone, C., El-Saloussy, K., Yu, C., & Rogers, C. A. (2014). “Design of steel sheathed cold-formed steel framed shear walls.” *Thin-Walled Structures*, *75*, 76-86.

Briere, V., and Rogers, C.A. (2017). “Higher capacity cold-formed steel sheathed and framed shear walls for mid-rise buildings: part 2”, Montréal, Canada: Department of Civil

Engineering and Applied Mechanics, McGill University (Research Report RP17-6).
DaBreo J, Balh N, Ong-Tone C, Rogers C.A. (2014) “Steel sheathed - cold-formed steel framed shear walls subjected to lateral and gravity loading.” *Thin-Walled Structures, 74*, 232-245.
Hutchinson, T.C., Wang, X., Hegemier, G., Meacham, B., Kamath, P., Sesma, F., and Holcomb, K. (2017). “Earthquake and Post-Earthquake Fire Performance of a Mid-Rise Cold-Formed Steel Framed Building.” *Proc., 2017 SEAOC Convention*, San Diego, CA.
Peterman, K. D., Stehman, M. J., Madsen, R. L., Buonopane, S. G., Nakata, N., and Schafer, B. W. (2016). “Experimental seismic response of a full-scale cold-formed steel-framed building. I: System-level response.” *Journal of Structural Engineering, 142*(12), 04016127.
Rizk, R., and Rogers, C.A. (2017). “Higher strength cold-formed steel framed / steel shear walls for mid-rise construction”, Montréal, Canada: Department of Civil Engineering and Applied Mechanics, McGill University (Research Report RP17-4).
Santos, V., and Rogers, C.A. (2017). “Higher capacity cold-formed steel sheathed and framed shear walls for mid-rise buildings: part 1”, Montréal, Canada: Department of Civil Engineering and Applied Mechanics, McGill University (Research Report RP17-5).
Schafer, B. W. (2011). “Cold-formed steel structures around the world: A review of recent advances in applications, analysis and design.” *Steel Construction*, 4(3), 141-149.
Serrette, R. (1997). “Behavior of Cyclically Loaded Light Gauge Steel Framed Shear Walls”. *Building to Last: Proceedings of Fifteenth Structures Congress*, Portland, OR.
Shamim, I., DaBreo, J., and Rogers, C. A. (2013). “Dynamic testing of single-and double-story steel-sheathed cold-formed steel-framed shear walls.” *Journal of Structural Engineering, 139*(5), 807-817.
Torabian, S., Nia, Z. S., and Schafer, B. W. (2016). “An Archetype Mid-Rise Building for Novel Complete Cold-Formed Steel Buildings.” *Wei-Wen Yu International Specialty Conference on Cold-Formed Steel Structures*, Baltimore, MD.
Wang, X.; Hutchinson, T. C., Hegemier, G., and Rogers, C. A. (2018). “Seismic Behavior of Cold-Formed Steel Shear Walls during Full-Scale Building Shake Table Tests”. *International Specialty Conference on Cold-Formed Steel Structures*, St. Louis, MO.
Yu, C., Vora, H., Dainard, T., and Veetvkuri, P. (2007). “Steel sheet sheathing options for CFS framed shear wall assemblies providing shear resistance.” Denton, USA: Department of Engineering Technology, University of North Texas (Report No. UNT-G76234).
Yu, C. (2010). “Shear resistance of cold-formed steel framed shear walls with 0.686 mm, 0.762 mm, and 0.838 mm steel sheet sheathing.” *Engineering Structures, 32*(6), 1522-1529.